Large eddy simulations of combustion instabilities in premixed flames

By C. Angelberger[1], D. Veynante[2], F. Egolfopoulos[3] AND T. Poinsot[4]

Our objective is to build a complete tool, based on large eddy simulations, to determine the forced response of a turbulent premixed burner, which is the missing information in models describing combustion instabilities. The developed code includes: (1) a chemistry model based on a new reduction technique (ICC) for propane and methane; (2) a flame thickening approach to handle flame turbulence interactions; and (3) specific boundary conditions to control and measure acoustic wave reflections on inlets and outlets. The chemistry reduction is derived and validated by comparison with full schemes/full transport results obtained from stagnation point flame codes. The flame thickening approach requires subgrid scale parameterization derived from flame/vortex interactions DNS. The code itself is a compressible parallel finite volume solver able to handle hybrid grids. The combustor forced response to acoustic wave excitations and to equivalence ratio modulations is compared in the geometry where experimental data are available (Poinsot *et al.*, 1987).

1. Motivations and objectives

Large eddy simulation (LES) is a promising tool to predict combustion instabilities in practical systems and to numerically test passive or active control techniques (McManus *et al.*, 1993). Flows submitted to such instabilities are controlled by very large eddies (Poinsot *et al.*, 1987; Candel *et al.*, 1996), and LES may be easier in these situations than in usual turbulent reacting flows where an extended range of eddies has to be incorporated to describe turbulence and chemistry interactions.

To satisfy emission regulations, modern gas turbines operate in very lean combustion regimes. These flames are extremely sensitive to combustion oscillations, but the exact phenomena leading to instabilities are still discussed. A central question is to determine the phenomena inducing unsteady reaction rates, required to sustain oscillations when an acoustic wave enters the combustion chamber. This effect may be due (at least) to two main effects. First, vortices formed in the combustion chamber may capture a large pocket of fresh gases burning only at later times in a violent process leading to high reaction rates. An acoustic wave propagating into feeding lines may also induce a local change of the equivalence ratio and, therefore, a modification of the burning rate. When the burner operates in a very lean

1 CERFACS, France
2 Laboratoire EM2C, CNRS and Ecole Centrale Paris, France
3 University of Southern California
4 Institut de Mecanique des Fluides de Toulouse and CERFACS, France

mode, non-flammable mixture pockets may enter the combustion zone, leading to extinction.

An important issue in combustion instabilities modeling is to choose between these two mechanisms: the first one requires a detailed computation of the flow field inside the chamber while the second one may be addressed with more global tools. Both may be studied together or separately using large eddy simulations. LES is used to examine which mechanism is predominant in the case of a backward facing step premixed burner developed at Ecole Centrale Paris (ECP) for which an extensive set of experimental results for the homogeneous case is available (Poinsot *et al.*, 1987). This configuration is also similar to many classical combustion instabilities experiments (for example Keller *et al.*, 1981) and multiple industrial devices. To achieve this objective, several tools were integrated:

• (1) An LES solver able to handle complex geometries. Various techniques have been previously proposed for LES in turbulent premixed combustion (see a review in Veynante and Poinsot, 1997a), but few of them have been used in a realistic configuration (see, for example, Kailasanath *et al.*, 1991). Real combustion chambers require meshes able to deal with highly complex geometries.

• (2) The choice of a proper chemical description remains a critical issue in reacting flows. Reduced chemical schemes able to predict changes in equivalence ratio for methane and propane are developed here using a new technique called ICC (Integrated Complex Chemistry), described in section 3.

• (3) Thermal boundary conditions at the walls of the combustion chamber control flame stabilization and quenching (Veynante and Poinsot 1997b). In the ECP burner, ceramic walls are assumed to be adiabatic (Poinsot *et al.*, 1987).

• (4) Combustion is handled using the thickened flame (TF) approach (section 4) initially proposed by O'Rourke and Bracco (1979) and tested by Veynante and Poinsot (1997b). As the thickened flame is more sensitive to strain than the real flame, TF approach and ICC methodology are coupled, requiring that the thickened flame behaves dynamically like the real thin flame.

2. Configuration and scope of present study

The generic configuration is displayed in Fig. 1. An acoustic wave traveling along the feeding line of a backward facing step combustor induces an air flow rate perturbation $\dot{m}'_a$ of the mean air flow rate $\dot{m}_a$ and a fluctuation $\dot{m}'_f$ of the mean fuel flow rate $\dot{m}_f$. The perturbation ϕ' of the mean equivalence ratio ϕ is given by:

$$\frac{\phi'}{\phi} = \frac{\dot{m}'_f}{\dot{m}_f} - \frac{\dot{m}'_a}{\dot{m}_a} \tag{1}$$

This perturbation influences burning rate, but the hydrodynamic perturbation, $\dot{m}'_a$, also induces the formation of a vortex near the chamber dump. These two effects may be isolated by performing the following simulations:

• Case A: Aerodynamical (or acoustic) forcing of the chamber. In this case the inlet flow rate fluctuates, keeping the equivalence ratio constant.

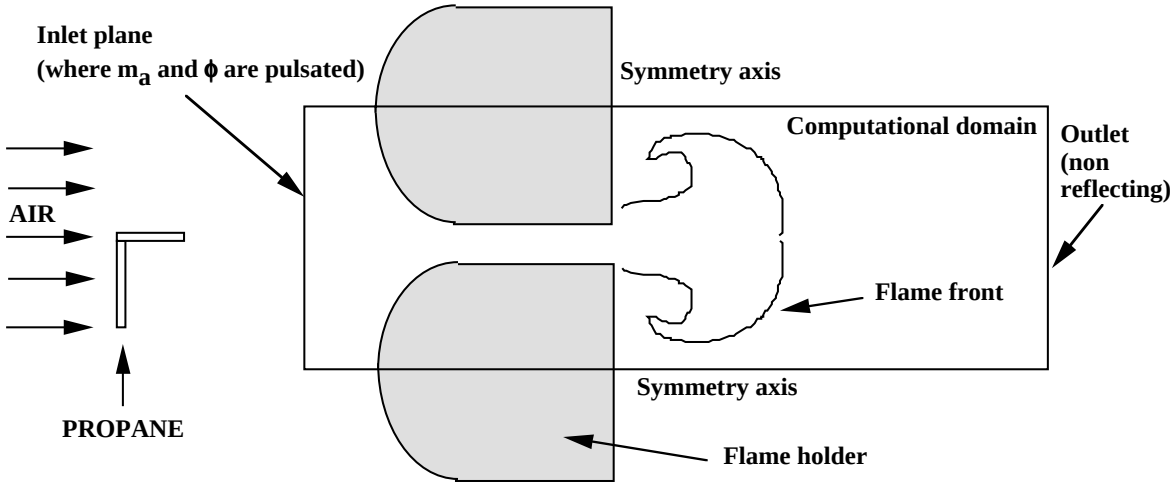

FIGURE 1. Configuration for simulations of combustion instabilities: the propane - air burner used by Poinsot *et al.* (1987). Only one of the injection slots is computed (the real system had five slots). The computational domain is 22.4 cm long and 2 cm high.

• Case C: Chemical forcing of the chamber (modulation of inlet equivalence ratio) without hydrodynamic forcing.

• Case F: Full forcing of the chamber. Obviously the real situation corresponds to a case where chemical and acoustic forcing are combined, but this case is not investigated here where only cases A and C are compared.

3. Reducing chemistry for LES: the ICC technique

Simplified kinetic schemes closely matching several flame properties for variable equivalence ratio are developed for lean methane/air and propane/air mixtures in the operating conditions of the ECP experiment (pressure $P = 1$ atm, fresh gases temperature $T_0 = 300$ K), using the ICC technique (Mantel *et al.*, 1996; Bedat *et al.*, 1997). Usually, one-step chemistry simplified schemes have been derived by only matching laminar flame speeds (Westbrook and Dryer, 1981). The ICC technique adds the constraint to match strain rates effects and to achieve numerical goals such as limitations of activation energies.

First, laminar flame speeds, flame structure, and the response to strain rate are determined in one-dimensional configurations using Chemkin-based codes and a detailed description of chemical kinetics and molecular transport to predict a reference case. The laminar flame speeds and flame structure (e.g. thickness) are determined through the one-dimensional PREMIX code (Kee *et al.*, 1985). For premixed flames, the response to strain rate includes the determination of extinction strain rates in the symmetric, twin-flame, opposed-jet configuration (fresh mixture counterflowing against an identical fresh mixture) and the variation of the spatially-integrated heat release with strain rate in the opposed-jet, fresh mixture against equilibrium

products configuration. This latter configuration is probably of dominant importance in turbulent premixed combustion, while the interaction of two streams of fresh mixtures may be of reduced but still non-negligible importance. On the other hand, experimental data are available for the twin-flame configuration (Law *et al.*, 1986) used as a data-base to test the ability of the detailed chemistry to predict extinction. Extinction strain rates are accurately determined by the opposed-jet code through the inclusion of one-point continuation (Egolfopoulos and Dimotakis, 1998), allowing for the description of turning-point behavior in the strain rate domain.

In a second part, similar simulations are conducting using simplified chemistry. The main goal is to "tune" the kinetic parameters to closely mimic several flame properties. Mantel *et al.* (1996) and Bedat *et al.* (1997) have shown that one-step global chemistry can predict flame propagation as well as flame extinction for a given fuel-to-air equivalence ratio, ϕ, tuning independently the pre-exponential factor A and the activation energy E_a. An important element of the ICC technique, compared to other reduction methods, is that the simplified chemistry is tested by modified versions of Chemkin-based codes, allowing for the use of simplified transport coefficients that are compatible with the ones used in the actual DNS or LES simulations. It has been found that results obtained by using simplified chemistry and detailed transport may be noticeably different compared to the ones obtained with simplified chemistry and simplified transport. Furthermore, thermal radiation from CO_2 and H_2O at the optically-thin limit (Egolfopoulos, 1994) are included. Thermal losses may be of particular importance on flame propagation and extinction (Law and Egolfopoulos, 1992; Egolfopoulos, 1994) in lean premixed combustion applications, such as gas turbines. Finally, the ICC technique produces kinetic schemes with relatively low level of stiffness, reducing thus the cost of DNS or LES simulations.

In the previous ICC studies, simplified chemical mechanisms were derived for a fixed equivalence ratio. The technique is extended here to account for variable equivalence ratio as well as for flame thickening. A one-step global chemistry model was derived, satisfactorily describing several flame properties of lean propane/air mixtures at $P = 1$ atm and $T_0 = 300$ K. The scheme is $C_3H_8 + 5O_2 \rightarrow 3CO_2 + 4H_2O$ with the specific reaction rate given by:

$$\dot{\omega} = A\,[C_3H_8]^a [O_2]^b exp(-E_a/RT)$$

where $[C_3H_8]$ and $[O_2]$ are the reactants molar concentrations, a and b the corresponding concentration exponents, A the pre-exponential factor, E_a the activation energy, R the gas constant, and T the absolute local gas temperature. The reference detailed chemistry for C_3H_8 was compiled by combining a C3 submechanism (Pitz and Westbrook, 1986) with the well-established C1-C2 GRI 2.1 mechanism (Bowman *et al.*, 1996). Two sets of parameters were finally kept for propane:

Set 1: $a = 1.0$, $b = 0.5$, $A = 1.60E09$ (cgs units), $E_a = 14,000$ (cal/mole).

Set 2: $a = 1.0$, $b = 0.5$, $A = 1.50E10$ (cgs units), $E_a = 20,000$ (cal/mole).

The use of concentration exponents as fitting parameters was essential to better describe variable equivalence ratio effects for a given set of Arrhenius parameters,

as suggested by Westbrook and Dryer (1981). E_a was kept at the lowest possible values to assure low stiffness and a thicker reaction zone. Accordingly, the flame thickening factor, F, required for LES is reduced compared to higher E_a schemes. For example, for Set 1 with $E_a = 14,000$ cal/mole a flame thickening factor $F = 4$ may be used in the LES while for Set 2 with $E_a = 20,000$ cal/mole, $F = 6 - 8$ is required for the same level of flame resolution. Although the flame thickening results in flames which are easily resolved by LES and with practically the same laminar flame speed, the thicker flames will be more susceptible to strain rate effects compared to the "real" thinner flames. Thus, by minimizing the flame thickening factor F, the strain rate effect discrepancy is minimized.

Figure 2 depicts the experimental (Vagelopoulos and Egolfopoulos, 1998) laminar flame speeds, s_l^0, for atmospheric, lean C_3H_8/air mixtures as well as the predictions obtained by using detailed chemical kinetics and transport and the proposed simplified scheme. The agreement is quite satisfactory. Extinction strain rates, κ_{ext}, were also determined for the twin-flame, opposed-jet configuration (Fig. 3). As expected, the predictions of κ_{ext} with $F = 4$ were found to be quite low compared to the $F = 1$ simulations, but still high compared to the $E_a = 14,000$ cal/mole scheme with $F = 8$. Representative comparison of the extinction response for $F = 1$ and $F = 4$ for a ϕ=0.9 flame is shown in Fig. 4 for the $E_a = 14,000$ cal/mole scheme. However, the flame response to strain rate for the fresh reactants against equilibrium products configuration, which is the prevailing one in the LES simulations, is in quite favorable agreement between the detailed and simplified chemistry simulations. The variation of the spatially integrated heat release rate with strain rate is shown in Fig. 5 for the detailed chemistry simulations as well as the simplified chemistry simulations with $F = 1$ and $F = 4$. Extinction is not possible for such a configuration, and the overall response of the $F = 4$ flames appears to be in close agreement with the detailed simulations.

4. Incorporating subgrid-scale effects into the thickened flame model

A complete description of the thickened flame (TF) model may be found for RANS models in Butler and O'Rourke (1977) and for LES models in Veynante and Poinsot (1997b). The key idea is to thicken the flame while maintaining its propagation speed. Following classical premixed laminar flame theories, this may be achieved simply by multiplying the thermal and molecular diffusivities a by a thickening factor F and dividing the preexponential constant A by the same factor F. With this transformation, the flame is thickened by a factor F and may be explicitly resolved on the LES mesh for sufficiently large values of F.

Unfortunately, when the flame is thickened from δ_l^0 to $F\delta_l^0$, the chemical time, estimated as $\tau_c = \delta_l^0/s_l^0$, becomes $F\tau_c$. Accordingly, the interaction between turbulence and chemistry may be modified because the Damköhler number, $Da = \tau_t/\tau_c$, comparing turbulent and chemical time scales is also decreased by a factor F. The interaction between flame and turbulence is altered in two main ways. First, eddies smaller than $F\delta_L^0$ do not interact with the flame any more, and their effects have to be incorporated in the modeling as a subgrid scale effect. Eddies larger than $F\delta_L^0$ interact with the flame front, but their efficiency may be affected.

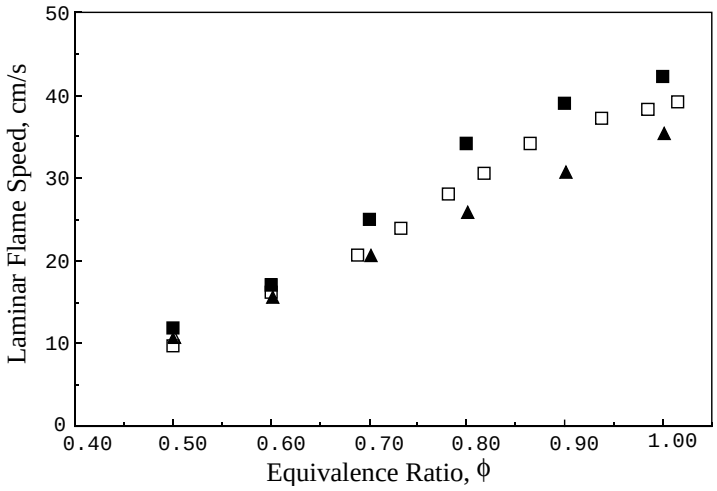

FIGURE 2. Variation of laminar flame speed with equivalence ratio for atmospheric C_3H_8/air mixtures (fresh gases initial temperature $T_0 = 300$ K). □ : experiments; ■ : predictions by detailed chemistry; ▲ : predictions by proposed simplified chemistry.

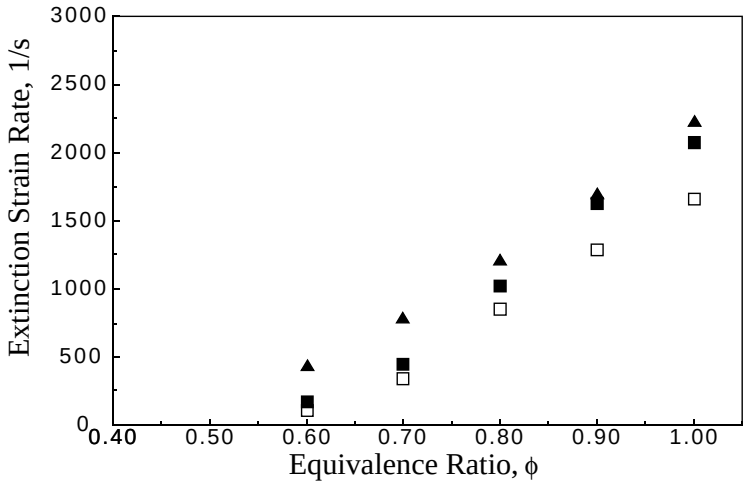

FIGURE 3. Variation of extinction strain rates κ_{ext} with equivalence ratio ϕ for atmospheric C_3H_8/air mixtures with reactants at initial temperature $T_0 = 300$ K, in the twin-flame, opposed-jet configuration. □ : experiments; ■ : predictions by detailed chemistry; ▲ : predictions by proposed simplified chemistry and $F = 1$.

4.1 DNS of flame/vortex interaction

Direct numerical simulation (DNS) of flame/vortex interactions is used to investigate how flame/turbulence interaction is affected by the thickening of the flame front and to propose a subgrid scale model to compensate these effects. A pair of counter-rotating vortices interacts with an initially planar laminar flame (Poinsot *et al.*, 1991). The ratio of the vortex size r to the initial flame thickness δ_l^0 is kept constant whereas three values of the vortex to laminar flame speeds ratio, v'^0/s_l^0,

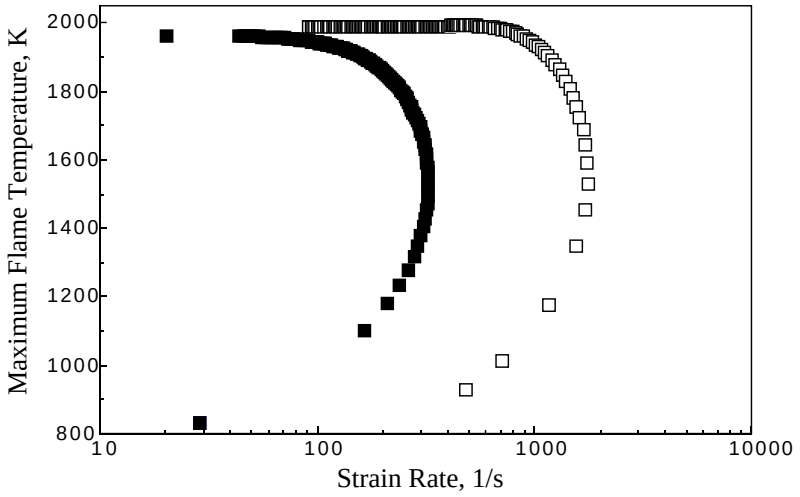

FIGURE 4. Variation of maximum flame temperature with strain rate for an atmospheric, $\phi = 0.9$ C_3H_8/air mixture (fresh gases initial temperature $T_0 = 300$ K), in the twin-flame, opposed-jet configuration. Predictions using the proposed simplified chemistry for $F = 1$ (□) and $F = 4$ (■).

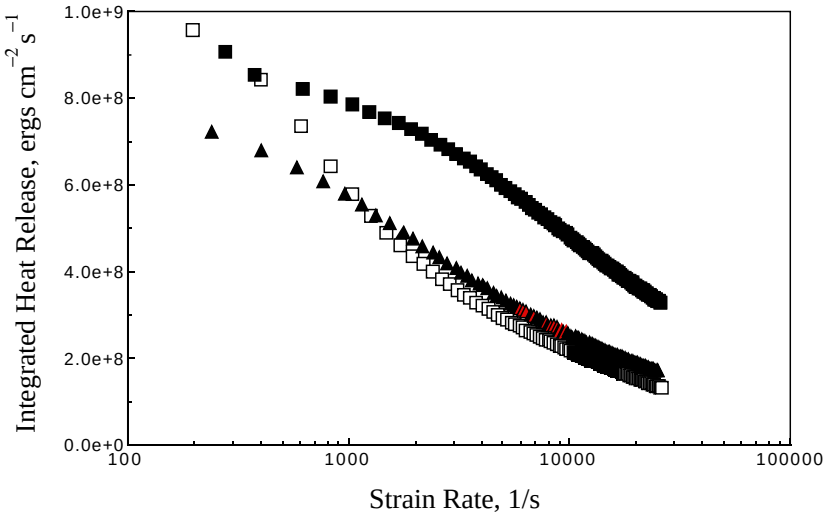

FIGURE 5. Variation of integrated heat release rate with strain rate for an atmospheric, $\phi = 0.9$ C_3H_8/air mixture with reactants at initial temperature $T_0 = 300$ K, in the fresh reactants against equilibrium products, opposed-jet configuration. □: predictions by detailed chemistry; ■: predictions by the proposed simplified chemistry and $F = 1$; ▲: predictions by the proposed simplified chemistry and $F = 4$.

are considered (cases A, B, and C). Five values of the thickening factor F are investigated (F = 1.0, 2.5, 5., 10., and 25.). Two additive cases (D1 and D2) are used to check the influence of the length scale ratio r/δ_l^0. Numerical parameters are summarized in Table I.

TABLE I: Flow conditions for DNS of flame/vortex interactions. For all flows: the acoustic Reynolds number Re_a is $= c_0 L/\nu_0 = 15000$; the temperature change through the flame front is $T_2/T_1 = 4$ ($\alpha = (T_2 - T_1)/T_2 = 0.75$); the sound speed in the fresh gas is c_0; the activation temperature T_a is such that $\beta = \alpha T_a/T_2 = 8$; the flame Mach number s_l^0/c_0 is 0.0159; δ_l^1 is the flame thickness after thickening ($\delta_l^1 = F\,\delta_l^0$). The initial flame thickness, δ_l^0, estimated from $\delta_l^0 s_l^0/\nu = 4$, is $\delta_l^0/L = 0.0168$. The vortex size, r, is estimated from the distance between the two vortex cores. v' measures the vortices velocity. The computational domain is $L_x \times L_y$, discretized on $N_x \times N_y$ grid points.

RUN	r/δ_l^0	v'^0/s_l^0	F	r/δ_l^1	L_x/L	L_y/L	N_x	N_y
A1	30.	8.	1.0	30.	3.	3.	1025	1025
A2	30.	8.	2.5	12.	6.	3.	801	401
A3	30.	8.	5.0	6.	3.	3.	201	201
A4	30.	8.	10.	3.	3.	3.	129	129
A5	30.	8.	25.	1.2	10.	3.	257	129
B1	30.	4.	1.0	30.	3.	3.	1025	1025
B2	30.	4.	2.5	12.	6.	3.	801	401
B3	30.	4.	5.0	6.	3.	3.	201	201
B4	30.	4.	10.	3.	3.	3.	129	129
B5	30.	4.	25.	1.2	10.	3.	257	129
C1	30.	0.8	1.0	30.	3.	3.	1025	1025
C2	30.	0.8	2.5	12.	6.	3.	801	401
C3	30.	0.8	5.0	6.	3.	3.	201	201
C4	30.	0.8	10.	3.	3.	3.	129	129
C5	30.	0.8	25.	1.2	10.	3.	257	129
D1	60.	8.	10.	6.	6.	6.	257	257
D2	60.	1.6	10.	6.	6.	6.	257	257

The temporal evolution of the total reaction rate and the corresponding values of the flame surface (estimated from the iso-surface $c^* = 0.8$ of the reaction progress variable) are plotted in Fig. 6 for Cases C1 to C5. As expected, as F is increased the total reaction rate decreases. Reduced values of the total reaction rate and total flame surface are in close agreement, showing that the local reaction rate is not affected by the thickening process whereas the vortices become unable to create flame surface by wrinkling.

Flame surface evolutions depend on the vortices-induced flame stretch $\langle\kappa\rangle_s$. Values of $\langle\kappa\rangle_s$, extracted from DNS as done by Meneveau and Poinsot (1991), are displayed in Fig. 7. As expected, $\langle\kappa\rangle_s$ increases with the vortex-induced strain rate v'/r and decreases with decreasing values of the length scale ratio r/δ_l^1 because vortices become inefficient (Poinsot *et al.*, 1991). For cases D1 and D2, the length scale ratio r/δ_l^0 corresponding to the actual flame is increased by a factor of 2 compared

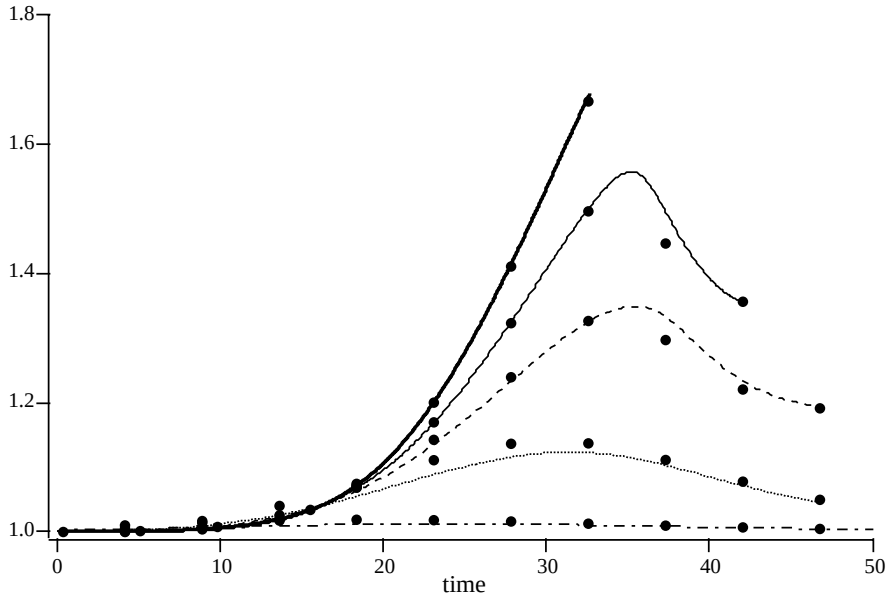

FIGURE 6. Total reaction rate versus time during flame vortex interaction for different values of the thickening factor F: cases C1 (——— , $F = 1.$), C2 (——— , $F = 2.5$), C3 (- - - - , $F = 5.$), C4 (····· , $F = 10.$) and C5 (— — — , $F = 25.$). Reaction rate values are made non-dimensional using the corresponding planar laminar flame quantities. Reduced flame surfaces are also plotted (•). Times are reduced using the flame time δ_l^0/s_l^0.

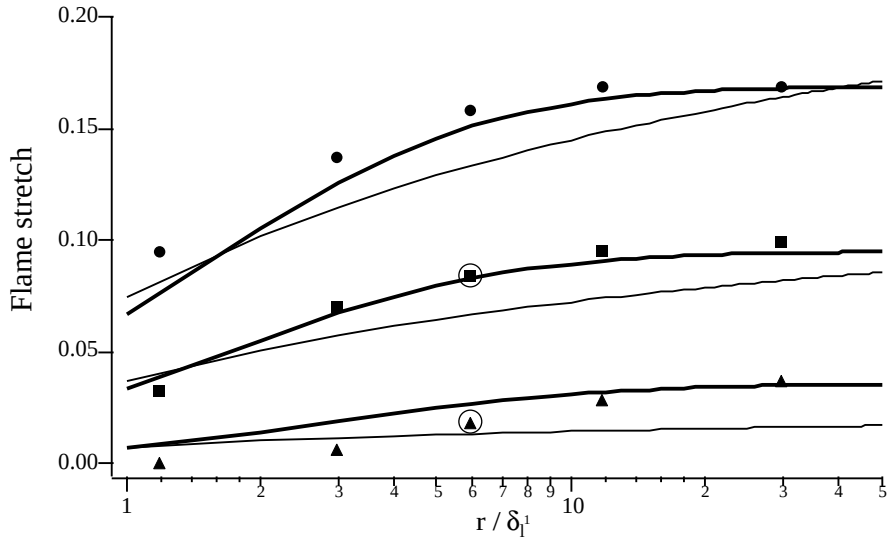

FIGURE 7. Flame stretch $\langle K \rangle$ induced by the pair of vortices plotted as a function of the length scale ratio r/δ_l^1 for cases An (•), Bn (■), Cn (▲), Dn (○). The bold solid line (———) corresponds to the proposed efficiency function C_n (Eq. 7). The efficiency function C_{MP} (Eq. 6) proposed by Meneveau and Poinsot (1991) is also plotted (———). Stretches are reduced using the flame characteristic time δ_l^0/s_l^0.

to previous cases. For case D1, the vortex-induced strain rate v'/r corresponds to cases B (whereas the maximum vortex velocity is the same as in cases A). The length scale ratio r/δ_l^1 is 6, and the stretch extracted from DNS corresponds to case B3 despite an increased value of the thickening factor F by a factor of 2. A similar result is found for case D2 having similar values of vortex induced strain rate, length scale ratio r/δ_l^1, and flame stretch as case C3.

To summarize our results, an increase of the flame thickening leads to a decrease of the flame front wrinkling because of a decreasing efficiency of vortices as length scale ratio r/δ_l^1 is decreased, as pointed out by Poinsot *et al.* (1991). The reduced efficiency of a vortex to wrinkle a flame front depends mainly on the value of r/δ_l^1 and not on the actual value of F (compare cases D1/B3 and D2/C3).

4.2 Estimation of the wrinkling of the flame front

A model incorporating the effects previously described should be based on the comparison between real and thickened flame wrinklings. Filtering the instantaneous flame surface density balance equation (Candel and Poinsot, 1990) leads to (Piana *et al.*, 1997; Boger *et al.*, 1998):

$$\frac{\partial \overline{\Sigma}}{\partial t} + \nabla.\left[\langle \mathbf{u} \rangle_s \overline{\Sigma}\right] + \nabla.\left[\langle w\mathbf{n} \rangle_s \overline{\Sigma}\right] = \langle \nabla.\mathbf{u} - \mathbf{nn} : \nabla\mathbf{u} \rangle_s \overline{\Sigma} + \langle w \nabla.\mathbf{n} \rangle_s \overline{\Sigma} = \langle \kappa \rangle_s \overline{\Sigma} \quad (2)$$

where $\overline{\Sigma}$ is the filtered flame surface density and corresponds to the subgrid scale flame surface. w is the flame front displacement speed, assumed here to be equal to the unstrained laminar flame speed s_l^0. $\mathbf{n}$ is the unit vector normal to the flame front pointing toward fresh gases, $\nabla.\mathbf{n}$ denotes the flame surface curvature, $a_T = \nabla.\mathbf{u} - \mathbf{nn} : \nabla\mathbf{u}$ corresponds to the strain rate induced by the flow field and acting on the flame front, and κ is the flame stretch. $\langle Q \rangle_s$ denotes averaging along the flame surface at the subgrid scale level. A complete analysis would require modeling and resolution of Eq. (2), but a simplified approach is proposed here. The subgrid scale surface averaged curvature $\langle \nabla.\mathbf{n} \rangle_s$ may be estimated as:

$$|\langle \nabla.\mathbf{n} \rangle_s| \approx \frac{1}{L_f} \approx \frac{1}{\alpha} \frac{\Xi - 1}{\Delta} \quad (3)$$

where L_f is the subgrid scale wrinkling length scale. Ξ is the wrinkling factor (i.e. the subgrid scale flame surface divided by its projection in the propagating direction) and Δ the filter size. α is a model constant of the order of unity. Assuming a subgrid scale equilibrium between flame surface and turbulence ($\langle \kappa \rangle_s \approx 0$), the wrinkling factor of the flame surface, Ξ, may be estimated as:

$$\Xi \approx 1 + \alpha \frac{\Delta}{s_l^0} \langle a_T \rangle_s \quad (4)$$

Estimating the subgrid scale strain rate as $\langle a_T \rangle_s \approx u'_\Delta/\Delta$, where u'_Δ is the subgrid scale turbulent velocity, leads to:

$$\Xi \approx 1 + \alpha \frac{\Delta}{s_l^0} \frac{u'_\Delta}{\Delta} = 1 + \alpha \frac{u'_\Delta}{s_l^0}, \quad (5)$$

recovering the wrinkling function (corresponding to the ratio of the subgrid scale turbulent flame speed $\overline{S}_T$ and the laminar flame speed s_l^0 used, for example, in the G-equation approach (Im *et al.*, 1997). The limited ability of small vortices to wrinkle the flame front must be parametrized and incorporated in a model for the strain rate $\langle a_T \rangle_s$ through an efficiency function as already done in RANS by Meneveau and Poinsot (1991) to derive the ITNFS (Intermittent Turbulent Net Flame Stretch) model.

4.3 Spectral analysis

Meneveau and Poinsot (1991) have modeled the effective strain rate induced by a pair of vortices (size r, velocity v') acting on a flame front as:

$$S_r = C_{MP}\left(\frac{r}{\delta_l^1}\right)\left[\frac{v'}{r}\right] = 10^{-c(s)}\left[\frac{v'}{r}\right] \quad with \quad c(s) = \frac{0.545}{log_{10}\left(\frac{4r}{\delta_l^1}\right) + 0.364} \tag{6}$$

where the efficiency function C_{MP} is only a function of the length scale ratio r/δ_l^1 whereas a clear dependence on the velocity ratio v'/s_l^0 is observed in our DNS. For example, cases A1 to A4 exhibit almost the same temporal evolution of the total reaction rate (not displayed here) whereas with a lower velocity ratio cases C1 to C4 lead to large differences (Fig. 6). A new efficiency function, compared to DNS data in Fig. 7, is then proposed:

$$C_n\left(\frac{r}{\delta_l^1}, \frac{v'}{s_l^0}\right) = \frac{1}{2}\left[1 + erf\left(0.6\, ln\left(\frac{r}{\delta_l^1}\right) - \frac{0.6}{\sqrt{\frac{v'}{s_l^0}}}\right)\right] \tag{7}$$

C_{MP}, also plotted on the figure, slightly underestimates the efficiency of small vortices and tends slowly toward its asymptotic value.

The effective strain rate due to a pair of vortices now has to be integrated over all length scales to estimate $\langle a_t \rangle_s$. Two cases are considered. First, a Heaviside efficiency function $C_H\left(r/\delta_l^c\right) = H\left(r - \delta_l^c\right)$, assuming that vortices lower than the cut-off length scale δ_l^c are unable to affect the flame, leads to a simple analytic solution. Then, the efficiency function C_n is considered. Meneveau and Poinsot have incorporated turbulence intermittency effects (various possible values of the velocity v' for a given vortex size r), but as these effects lead only to a weak modification of the final results, compared to modeling uncertainties they are not considered in the following to simplify numerical integrations. Assuming a homogeneous and isotropic turbulence, velocity v' and length r' scales are related:

$$v' = \left(\frac{r}{l_t}\right)^{\frac{1}{3}} u' = \left(\frac{r}{\Delta}\right)^{\frac{1}{3}} u'_\Delta \tag{8}$$

where l_t is the turbulence integral length scale, corresponding to the velocity u'. Then, following Meneveau and Poinsot (1991):

$$\langle a_T \rangle_s = \frac{0.28}{ln(2)} \int_{scales} C\left(\frac{r}{\delta_l^1}, \frac{v'}{s_l^0}\right) \frac{v'}{r}\, d\left[ln\left(\frac{l_t}{r}\right)\right] \tag{9}$$

leading to:

$$\langle a_T \rangle_s = \frac{0.28}{ln(2)} \frac{u'_\Delta}{\Delta} \left(\frac{\Delta}{l_t}\right)^{\frac{2}{3}} \int_{max\left[ln\left(\frac{l_t}{\Delta}\right),0\right]}^{ln\left(\frac{l_t}{\eta_k}\right)=\frac{3}{4}ln(Re)} C\left(\frac{l_t}{\delta_l^1}e^{-p}, \left(\frac{l_t}{\Delta}\right)^{\frac{1}{3}} \frac{u'_\Delta}{s_l^0} e^{-\frac{p}{3}}\right) e^{\frac{2}{3}p}\, dp \tag{10}$$

where η_k is the Kolmogorov length scale, and $Re = l_t u'/\nu \approx 4(l_t/\delta_l^0)(u'/s_l^0)$ the turbulence Reynolds number. The integration is performed on all length scales lower than the filter size Δ.

For a Heaviside efficiency function C_H, $\langle a_T \rangle_s$ has an analytical expression:

- a) For $\delta_l^c \leq \eta_k$: $$\langle a_T \rangle_s = \frac{0.42}{ln(2)} \frac{u'_\Delta}{\Delta} \left[\left(\frac{\Delta}{l_t}\right)^{\frac{2}{3}} Re^{1/2} - 1\right] \tag{11}$$
- b) For $\eta_k \leq \delta_l^c \leq \Delta \leq l_t$: $$\langle a_T \rangle_s = \frac{0.42}{ln(2)} \frac{u'_\Delta}{\Delta} \left[\left(\frac{\Delta}{\delta_l^c}\right)^{\frac{2}{3}} - 1\right] \tag{12}$$

Of course, if $\Delta \leq \delta_l^c$, $\langle a_T \rangle_s = 0$. If $\Delta \geq l_t$, Δ should be replaced by l_t in the previous expressions. In case b, corresponding to the general case, the strain rate depends only on local quantities for a given cut-off scale δ_l^c.

For the efficiency function C_n (Eq. 7), the integration is performed numerically, and the reduced strain rate $\Gamma_n = \langle a_T \rangle_s \Delta / u'_\Delta$ is plotted in Fig. 8. Γ_n increases with Δ/δ_l^1, contrary to the result expected from expressions (11) and (12) (Heaviside efficiency function), because Δ/δ_l^1, Δ/l_t and u'_Δ/s_l^0 are related. An increase of Δ/δ_l^1 corresponds to an increase of the turbulence Reynolds number Re. As the dependence of Γ_n with l_t/Δ is weak compared to the model uncertainties, Γ_n may be fitted by:

$$\Gamma_n\left(\frac{\Delta}{\delta_l^1}, \frac{u'_\Delta}{s_l^0}\right) = 0.75\, exp\left[-\frac{1.2}{\left(u'_\Delta/s_l^0\right)^{0.3}}\right] \left(\frac{\Delta}{\delta_l^1}\right)^{\frac{2}{3}} \tag{13}$$

which is in close agreement with the numerical integration of Γ_n as shown in Fig. 8. For comparison, Γ_{MP} estimated from the efficiency function C_{MP} (Eq. 6) is also displayed. Γ_{MP} is almost independent of the velocity ratio u'_Δ/s_l^0 (the only dependence comes through the turbulence Reynolds number and remains weak, as already pointed out by Meneveau and Poinsot, 1991) and depends weakly on the length scale ratio l_t/δ_l^1, as Γ_n.

4.4 Comments and practical implementation

Following the previous analysis, the wrinkling of the subgrid scale flame front may be estimated as:

$$\Xi = 1 + \alpha\Gamma\left(\frac{\Delta}{\delta_l^1}, \frac{u'_\Delta}{s_l^0}\right) \frac{u'_\Delta}{s_l^0} \tag{14}$$

This expression may also be used in a G-equation formalism (Im *et al.*, 1997) to estimate the subgrid scale turbulent flame speed or in a flame surface density approach (Boger *et al.*, 1998). A dynamic formulation could also be derived.

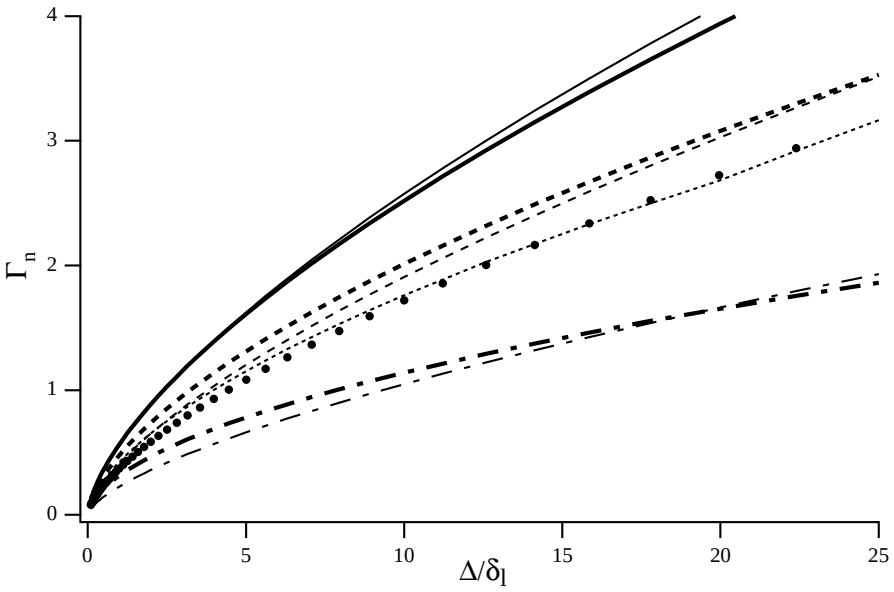

FIGURE 8. Reduced strain rate $\Gamma_n = \langle a_T \rangle_s \Delta / u'_\Delta$ versus the length scale ratio Δ/δ_l^1 estimated from the efficiency function C_n (Eq. 7). Γ_n is plotted for $l_t/\delta_l^1 = 100$ with $u'_\Delta/s_l^0 = 100$ (———), $u'_\Delta/s_l^0 = 10$ (- - - -) and $u'_\Delta/s_l^0 = 1$ (—- —-). Bold lines are obtained from numerical integrations of Eq. (10) whereas thin lines correspond to the proposed fit (Eq. 13). Γ_n is also plotted for case $l_t/\delta_l^1 = 20$ and $u'_\Delta/s_l^0 = 10$ (·····). Γ_{MP} (———), estimated from the efficiency function C_{MP} (Eq. 6) proposed by Meneveau and Poinsot, is displayed for comparison (• , $l_t/\delta_l^1 = 100$; $u'_\Delta/s_l^0 = 10$).

For a given turbulence and using Eq. (12), Ξ may be recast as:

$$\Xi = 1 + 0.42 \frac{\alpha}{ln(2)} \frac{u'}{s_l^0} \left(\frac{\Delta}{l_t}\right)^{\frac{1}{3}} \left[\left(\frac{\Delta}{\delta_l^c}\right)^{\frac{2}{3}} - 1\right] \tag{15}$$

For a thin flame front (i.e. $\Delta >> \delta_l^c$), Ξ increases linearly with Δ in a log-linear diagram and reaches a constant value when $\Delta \geq l_t$. This finding is in agreement with the experimental data obtained by Piana *et al.* (1997).

With a thickened flame, the actual wrinkling of the flame front is underestimated by an efficiency factor $E = \Xi\left(\delta_l^0\right)/\Xi\left(\delta_l^1\right)$. In practical applications, Δ is lower than the thickness δ_l^1. Accordingly, the thickened flame will not be wrinkled by subgrid scale turbulence and $\Xi\left(\delta_l^1\right) \approx 1$. The underestimation of the flame front wrinkling by the thickened flame approach should be corrected by increasing the flame speed by the efficiency factor E. This could be achieved by increasing the pre-exponential factor by a factor E^2 as done here, but the flame thickness may be kept constant by multiplying both the pre-exponential factor and the molecular and thermal diffusivities by a factor E. In this case, a subgrid scale diffusivity,

depending on the flame characteristics, is introduced. E is estimated here from:

$$E \approx \Xi\left(\delta_l^0\right) \approx 1 + \alpha\Gamma\left(\frac{\Delta}{\delta_l^0}, \frac{u'_\Delta}{s_l^0}\right)\frac{u'_\Delta}{s_l^0} \approx 1 + \alpha\Gamma\left(\frac{\Delta}{\delta_l^0}, \frac{u'_\Delta}{s_l^0}\right) C_s \frac{\Delta}{s_l^0}\sqrt{2S_{ij}S_{ij}}$$

where C_s is a model constant used in the estimate of u'_Δ from S_{ij}:

$$S_{ij} = \frac{1}{2}\left(\frac{\partial \widetilde{u}_i}{\partial x_j} + \frac{\partial \widetilde{u}_j}{\partial x_i}\right)$$

In the present preliminary tests, we use $\alpha\,\Gamma\,C_s = 0.1$.

To summarize, the thickening of the flame has two main effects:

• eddies smaller than $F\delta_L^0$ do not interact with the flame any more, and their effects have to be incorporated at the subgrid scale level using an efficiency factor E. Our preliminary results show that neglecting the efficiency function (i.e. $E = 1$, assuming a plane laminar subgrid scale flame) leads to an unexpected blow-off. In fact, the global reaction rate is underestimated, and the predicted flame becomes unable to sustain the incoming fresh gases flow.

• eddies larger than $F\delta_L^0$ interact with the flame front, but their efficiency may also be affected as described in Section 4.1. This effect was not incorporated here, but could be corrected by estimating an efficiency function at a test level $\widehat{\Delta} \approx 10F\delta_L^0$, corresponding to the size of the larger vortices affected by the flame front (see Fig 7).

5. Full simulations of the Ecole Centrale burner with no acoustic forcing

Simulations of the unforced flow in the ECP burner are performed using the AVBP code, a CFD package built on COUPL (CERFACS and Oxford University Parallel Library). AVBP has been used for a variety of unsteady flows in DNS and LES (Nicoud *et al.*, 1996; Nicoud, 1997; Ducros *et al.*, 1997). AVBP can handle hybrid meshes and is fully parallel. The previous models for chemistry and flame turbulence interaction were incorporated into this code and tested separately. Then, computations for the ECP burner were started for the operating conditions summarized in Table II. Propane combustion is modeled using chemistry parameters described in Section 3 (Set 2 with a thickening factor $F = 8$).

Table II. Physical parameters for the Ecole Centrale Paris burner simulation

Inlet temperature	Equivalence ratio	Inlet velocity	Flame speed	Adiabatic flame temperature
300 K	1	6.4 m/s	0.36 m/s	2190 K

All computations were performed in two dimensions since flow visualizations have indicated that large scale structures produced in this chamber were indeed two-dimensional. Common numerical parameters for all computations are described in

Table III. For all cases, the combustion chamber is computed as an amplifier system (and not as a resonator): inlet and outlet boundary conditions are non reflecting, and all acoustic waves produced in the combustor are allowed to leave the chamber so that no self-induced low-frequency mode can occur. The combustor may be forced to study its response. Forcing is introduced at the inlet of the combustor by modulating the incoming acoustic wave or the incoming gas equivalence ratio following the NSCBC technique (Poinsot and Lele, 1992).

Table III. Numerical parameters for the Ecole Centrale Paris burner simulation

Total number of points	LES model	Time Advancement	Range of Mesh size	CFL limit	F
41000	Filtered Smagorinski	RK3	0.07-0.3 mm	0.5	8

Typical simulations run during 500000 iterations, corresponding to 100 acoustic travel times in the chamber and more than 4 convective times. Initialization of computations in such cases is not simple since the LES code has very low levels of dissipation. The overall procedure used here is the following:

• Starting phase: the computation starts from an initial state where a strip of fresh gas is located in the combustion chamber and surrounded by two strips of burnt gas on each side. To allow stabilization during this first phase, fourth-order artificial viscosity is used.

• Transition phase: when the flow is established, artificial viscosity levels are reduced to negligible values, and the LES viscosity μ_t picks up while the flow becomes unsteady. Maximum values of the ratio μ_t/μ_{lam} (where μ_{lam} is the laminar viscosity in the fresh gases) are of the order of 20. The mean value of μ_t/μ_{lam} over the whole domain, however, is of the order of 0.3, showing that μ_t is distributed very intermittently.

• Measurement phase: after a few transit times in the burner, the mean flow is established, and measurements can be performed (with or without forcing).

In the absence of forcing, the flow stabilizes around a mean regime where two types of oscillations are observed. Small scale vortices are shed on the jet and propagate downstream. These vortices were also observed in the experiment (Zikikout, 1986). The frequency observed in the LES is of the order of 5 kHz while the measurements gave values closer to 3.8 kHz. Large scale movements of the reacting jet are also visible, both on the sinuous and varicose modes. These movements diminish as time goes by because the acoustic activity in the cavity decreases.

A typical snapshot of the flow for this regime is given in Fig. 9. The flame is only slightly corrugated and corresponds to the state observed in the experimental set-up in the absence of instabilities (Fig. 6 in Poinsot *et al.*, 1987).

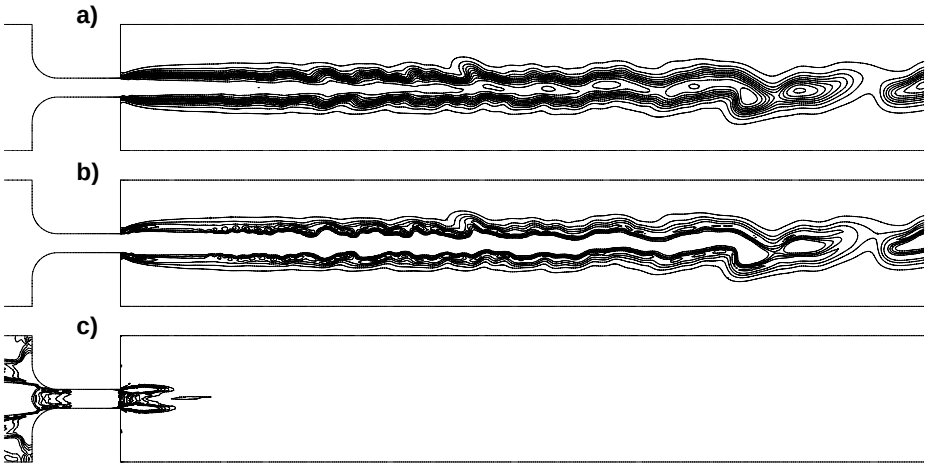

FIGURE 9. Instantaneous fields of temperature (a), reaction rate (b), and subgrid scale turbulent velocity (c) for an unforced regime.

6. Forced response of the Ecole Centrale burner

6.1 Response to an acoustic perturbation (Case A)

The objective is to reproduce the combustor response to a 530 Hz excitation of the inlet flow rate corresponding to one of the strongest instability modes observed in the ECP burner. More precisely, LES is used to measure the time delay between inlet flow rate perturbations and reaction rate oscillations. This delay was experimentally found to be close to 0.9 ms (Fig. 12 in Poinsot *et al.*, 1987). The wave amplitude is chosen to induce a flow rate change equal to 50 percent of the mean flow rate. Snapshots of temperature and reaction rate during one cycle of forcing are displayed respectively in Figs. 10 and 11.

The general features observed in the LES match those observed in the experiment: a large mushroom-shaped structure is produced (similar to vortices observed in impulsively-started jets) and leads to a high increase of flame surface and reaction rate. Fig. 12 displays time variations of inlet flow rate and heat release. The reaction rate lags the inlet flow rate by approximately 0.9 ms as observed in the experiment. The experimental heat release is also displayed, and a very good agreement on phases is obtained. Note that amplitudes cannot be compared because the experimental data contained only normalized values.

6.2 Response to a change in equivalence ratio (Case C)

In a second step, the combustor was forced by modulating the inlet equivalence ratio ϕ between 0.3 and 1.7 using a sinusoidal function (frequency 530 Hz). A large modulation amplitude is chosen to maximize the effects. To achieve such levels, both fuel and air flow rates would have to be affected by the acoustic wave in opposite directions. Since this is unlikely to happen in practice, the present simulations provide a maximization of potential effects of unmixedness on combustor response.

As the overall mass flow rate was kept constant, no vortices were formed at the inlet, and only the chemistry effects are observed. Fig. 13 (fuel mass fraction) and

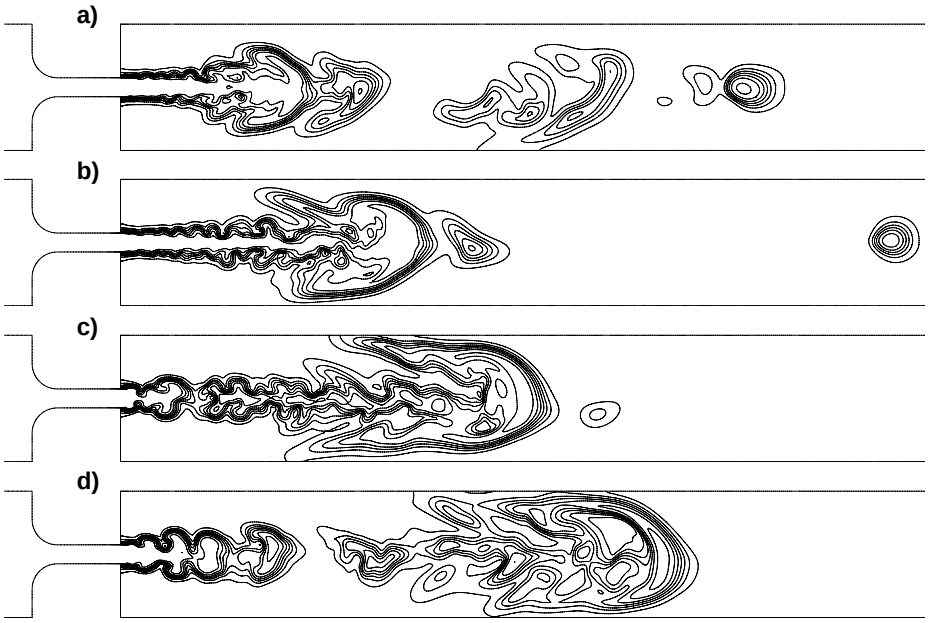

FIGURE 10. Temperature fields during one forcing cycle at 530 Hz. The time separation between each picture corresponds to a quarter period (0.47 ms)

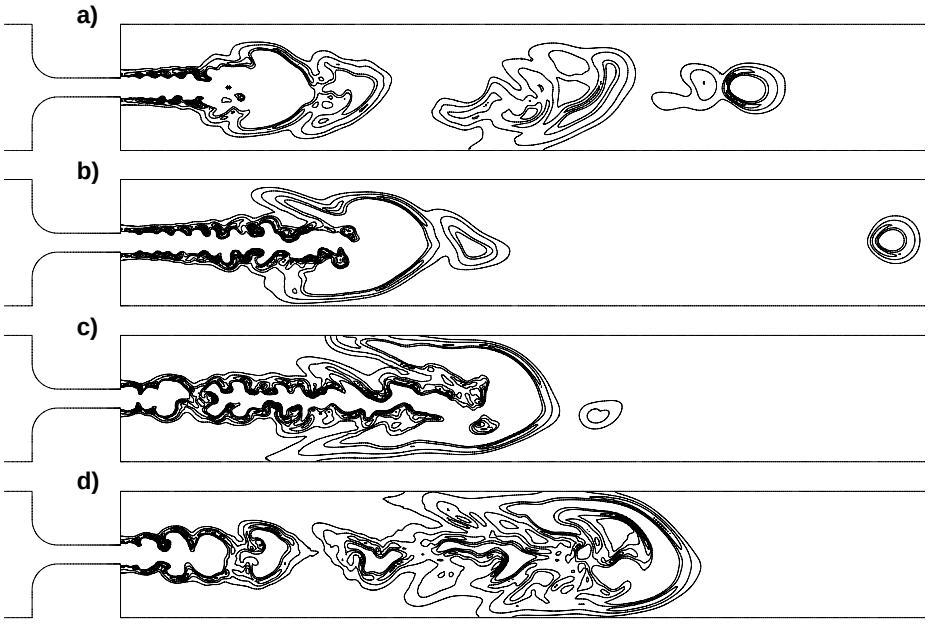

FIGURE 11. Reaction rate fields during one forcing cycle at 530 Hz.The time separation between each picture corresponds to a quarter period (0.47 ms)

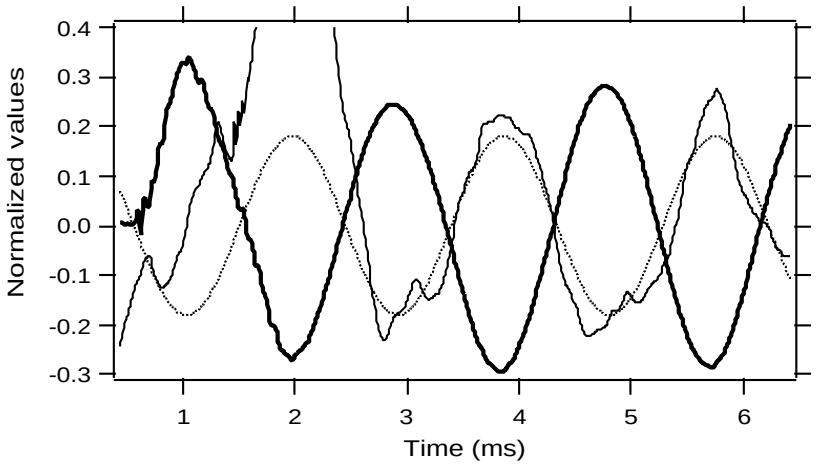

FIGURE 12. Time evolutions of inlet flow rate (——), window-integrated reaction rate in the LES (——) and in the Poinsot *et al.* experiment (- - - -).

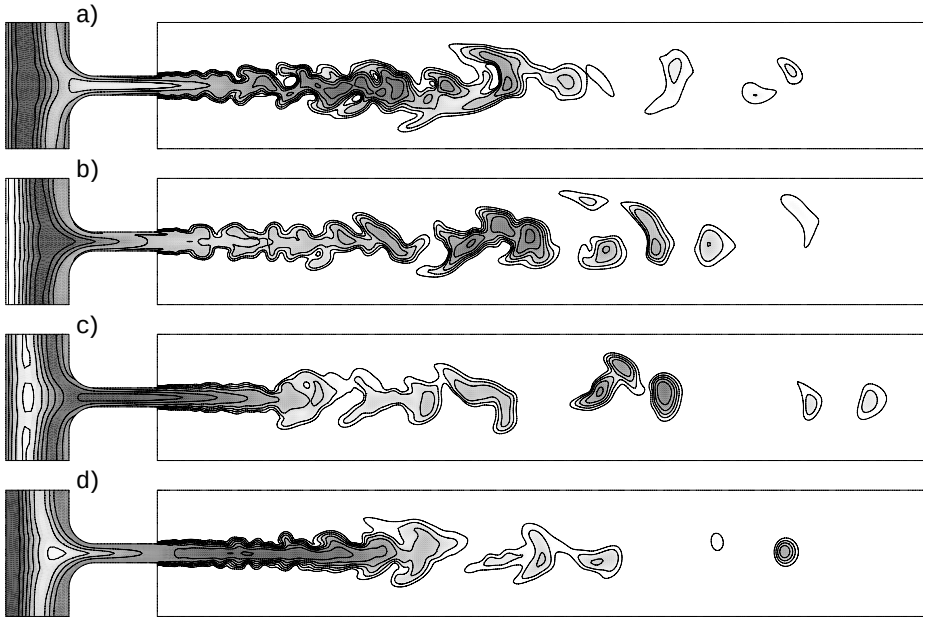

FIGURE 13. Fuel mass fraction fields during one forcing cycle of the equivalence ratio ϕ at 530 Hz. Dark and white regions correspond respectively to rich ($\phi = 1.7$) and lean ($\phi = 0.3$) gases.

Fig. 14 (reaction rate) show how the lean and rich regions created at the inlet enter the combustor and affect the flame front.

The total reaction rate is modified by the pulsation of the inlet fuel mass fraction as shown in Fig. 15: the inlet fluctuations of fuel mass fraction are slightly damped before entering the combustor (because they pass through the convergent), but combustion is modulated by these perturbations.

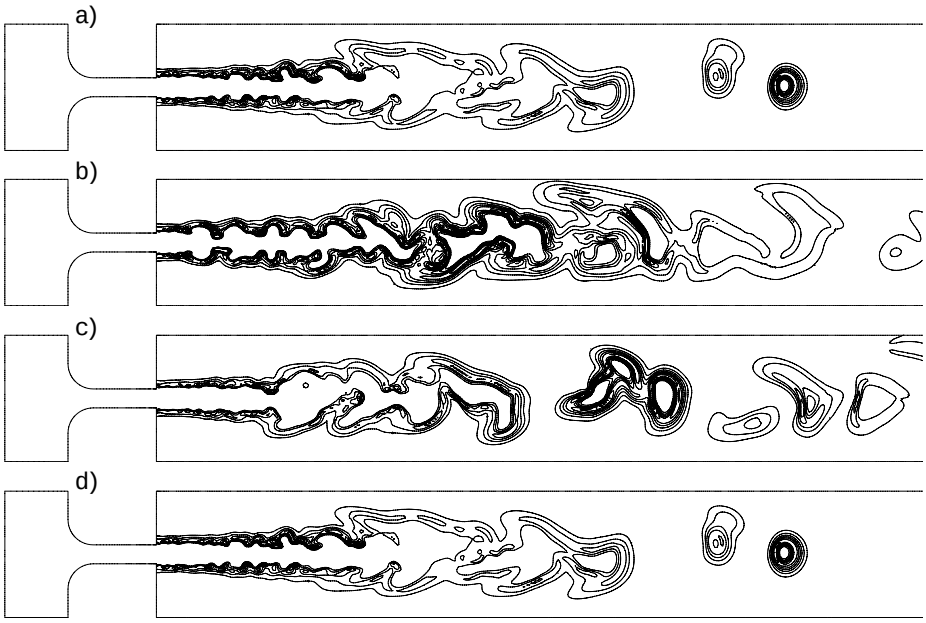

FIGURE 14. Reaction rate fields during one forcing cycle at 530 Hz (modulation of equivalence ratio ϕ).

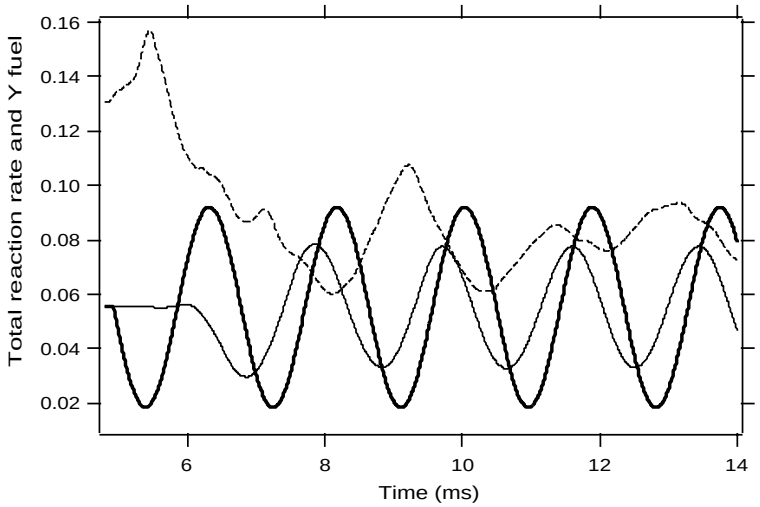

FIGURE 15. Fuel mass fraction at the inlet of the domain (premixing chamber) (———), in the jet at the dump section (———), and total reaction rate (- - - -).

Finally, Fig. 16 compares the effects of acoustic forcing (case A) with those of chemical forcing (Case C). The case without forcing is added for reference. Obviously, runs should be continued to confirm this analysis, but it appears that acoustic forcing has a stronger effect on the total reaction rate than chemical forcing. Since we chose a very large range of variations for the chemical forcing, it seems that acoustic forcing is the main phenomenon to consider for combustion instabilities in the present system.

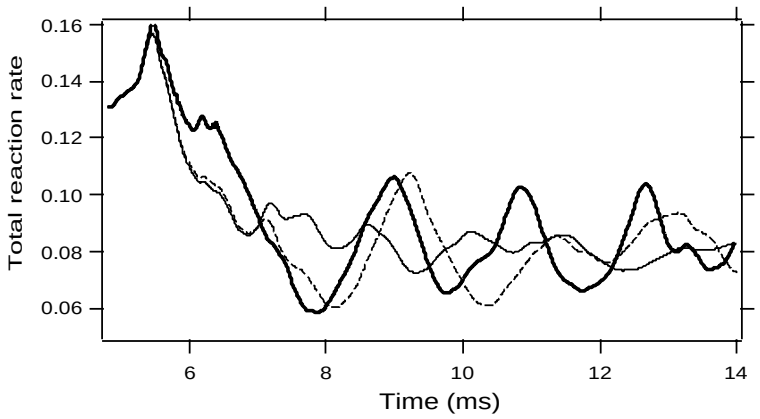

FIGURE 16. Total reaction rate vs time for unforced flow (———), acoustic forcing at 530 Hz with an amplitude of 50 percent (———) and for a modulation of equivalence ratio between 0.3 and 1.7 (- - - -).

7. Conclusion

Large eddy simulations of the effects of acoustic waves and equivalence ratio variations on flame response have been performed for a premixed turbulent flame stabilized in a backward-facing step combustor. The developed code includes: (1) a chemistry model based on a new reduction technique, ICC, for propane and methane; (2) a flame thickening methodology, incorporating subgrid scale modeling, to handle flame turbulence interactions; and (3) specific boundary conditions to control and measure acoustic wave reflections on inlets and outlets. The code itself is a compressible parallel finite volume solver able to handle hybrid grids (AVBP).

Results indicate that the final tool was able to predict forced combustor response over many excitation cycles and to reproduce the phenomena observed in the experiment of Ecole Centrale Paris. The phase between flow rate oscillations and unsteady heat release, for example, was recovered in the case of acoustic forcing. Modulating the inlet equivalence ratio also led to unsteady heat release but with lower amplitudes than with acoustic forcing.

Numerical simulations were carried out at IDRIS (Institut du Développement et des Ressources en Informatique Scientifique, Orsay, France).

REFERENCES

BEDAT B., EGOLFOPOULOS F. ET POINSOT T. 1997 Integrated Combustion Chemistry (ICC) for Direct Numerical Simulations: Application to premixed and non-premixed combustion. *Western States Section Meeting of the Combustion Institute*, Los Angeles, Paper WSS/CI 97F-122.

BOGER, M., VEYNANTE, D., BOUGHANEM, H. & TROUVÉ T. 1998 Direct numerical simulation analysis of flame surface density concept for large eddy simulation of turbulent premixed combustion. *27^{th} Symp. (Int.) on Combustion.*

The Combustion Institute, Pittsburgh.

Bowman, C.T., Frenckclack, M, Gardiner, W. & Smith, G. 1996 The GRI 2.1 Mechanism. *Personal Communication.*

Butler T.D. & O' Rourke P.J. 1977 *16th Symp. (Int.) on Combustion*, The Combustion Institute, Pittsburgh, 1503-1515.

Candel, S. & Poinsot, T. 1990 Flame stretch and the balance equation for the flame area. *Comb. Sci. Tech.* **70,** 1.

Candel, S., Huynh, C. & Poinsot, T. 1996 Unsteady combustion. *Nato ASI Series*, Kluwer Academic Publishers, Dordrecht. 83-112.

Ducros, F., Nicoud, F. and Schönfeld, T. 1997 Large Eddy Simulations of compressible Flows on Hybrid Meshes. *11th Symp. on Turbulent Shear Flows*, Grenoble, France.

Egolfopoulos F.N. 1994 Geometric and Radiation Effects on Steady and Unsteady Strained Laminar Flames. *25th Symp. (Int.) on Combustion*, The Combustion Institute, Pittsburgh, 1375-1381.

Egolfopoulos F.N. & Dimotakis P.E. 1998 Non-Premixed Hydrocarbon Ignition at High Strain Rates. *27th Symp. (Int.) on Combustion*, The Combustion Institute, Pittsburgh.

Law C.K. & Egolfopoulos F.N. 1992 A Unified Chain-Thermal Theory of Fundamental Flammability Limits. *24th Symp. (International) on Combustion*, The Combustion Institute, Pittsburgh, 137-144.

Im, H.G., Lund, T. & Ferziger, J. 1997 Large eddy simulation of turbulent front propagation with dynamic models. *Phys. Fluids A.* **9,** 3826-3833.

Kailasanath, K., Gardner, J. H., Oran, E. S. & Boris, J. P. 1991 Numerical simulations of unsteady reactive flows in a combustion chamber. *Comb. Flame.* **86,** 115-134.

Kee, R. J., Grcar, J. F., Smooke, M. D. & Miller J. A. 1985 A Fortran Program for Modeling Steady Laminar One-Dimensional Premixed Flames. *Sandia Report SAND85-8240.*

Keller, J. O., Vaneveld, L., Korschelt, D., Hubbard, G. L., Ghoniem, A. F., Daily, J. W. & Oppenheim, A. K. 1981 Mechanism of instabilities in turbulent combustion leading to flashback. *AIAA J.* **20,** 254-262.

Law, C.K., Zhu, D.L. & Yu, G. 1986 Propagation and extinction of stretched premixed flames. *21st Symp. (Int.) on Combustion*, The Combustion Institute, Pittsburgh, 1419-1426.

Mantel, T., Egolfopoulos F. and Bowman, C.T. 1996 A new methodology to determine kinetic parameters for one- and two- step chemical models. *Stanford CTR Summer Program 1996*, Center for Turbulence Research, NASA Ames/Stanford Univ., 137-149.

McManus, K., Poinsot, T. &Candel, S. 1993 A review of active control of combustion instabilities. *Prog. Energy Comb. Sci.* **19,** 1-29.

MENEVEAU, C. & POINSOT, T. 1991 Stretching and quenching of flamelets in premixed turbulent combustion. *Comb. Flame.* **86,** 311-332.

NICOUD, F., DUCROS, F., SCHÖNFELD, T. 1996 Towards Direct and Large Eddy Simulations of compressible Flows in complex geometries. *5th French-German Workshop*, Munich.

NICOUD, F. 1997 Effects of strong wall injection on the structure of a low-Reynolds turbulent flow. *Submitted to Int. J. Num. Meth. Fluids.*

PIANA, J., DUCROS, F. & VEYNANTE, D. 1997 Large eddy simulations of turbulent premixed flames based on the G equation and a flame front wrinkling description. *11^{th} Symp. on Turbulent Shear Flows*, Grenoble, France.

PITZ, W. J. & WESTBROOK, C. K. 1986 Chemical Kinetics of the High Pressure Oxidation of n-Butane and its Relation to Engine Knock. *Combust. Flame.* **63,** 113-133.

POINSOT, T., TROUVÉ, A., VEYNANTE, D., CANDEL, S. & ESPOSITO, E. 1987 Vortex driven acoustically coupled combustion instabilities. *J. Fluid Mech.* **177,** 265-292.

POINSOT, T. & LELE, S. 1992 Boundary conditions for direct simulations of compressible viscous flows. *J. Comp. Physics.* **101,** 104-129.

POINSOT, T., VEYNANTE, D., CANDEL, S. 1991 Quenching processes and premixed turbulent combustion diagrams. *J. Fluid Mech.* **228,** 561-606.

O'ROURKE, P.J. & BRACCO, F.V. 1979 Two scaling transformations for the numerical computation of multidimensional unsteady laminar flames. *J. Comp. Physics.* **33,** 2, 185-203.

TROUVÉ, A. & POINSOT, T. 1994 The evolution equation for the flame surface density. *J. Fluid Mech.* **278,** 1-31.

VAGELOPOULOS C.M. & EGOLFOPOULOS F.N. 1998 Direct Experimental Determination of Laminar Flame Speeds. *27^{th} Symp. (International) on Combustion.* The Combustion Institute, Pittsburgh.

VEYNANTE, D. & POINSOT, T. 1997a Reynolds-averaged and Large Eddy Simulation modeling for turbulent combustion. In *New tools in turbulence modeling,* O. Metais and J. Ferziger Eds, Les Editions de Physique.

VEYNANTE, D. & POINSOT, T. 1997b Large Eddy Simulation of combustion instabilities in turbulent premixed burners. *Annual Research Briefs*, Center for Turbulence Research, NASA Ames/Stanford Univ., 253-274.

WESTBROOK, C. AND DRYER, F. 1981 Simplified Reaction Mechanism for the Oxidation of Hydrocarbon Fuels in Flames. *Comb. Sci. Tech.* **27,** 31-43.

ZIKIKOUT, S., CANDEL, S., POINSOT, T., TROUVÉ, A.& ESPOSITO, E. 1986 High frequency oscillations produced by mode selective acoustic excitation. *21^{st} Symp. (Int.) on Combustion*, The Combustion Institute, Pittsburgh.